

# PanoFlow: Learning Optical Flow for Panoramic Images

Hao Shi<sup>†1,5</sup>, Yifan Zhou<sup>†2</sup>, Kailun Yang<sup>3</sup>, Yaozu Ye<sup>1</sup>, Xiaoting Yin<sup>1</sup>, Zhe Yin<sup>4</sup>, Shi Meng<sup>5</sup>, and Kaiwei Wang<sup>1</sup>

**Abstract**—Optical flow estimation is a basic task in self-driving and robotics systems, which enables to temporally interpret the traffic scene. Autonomous vehicles clearly benefit from the ultra-wide Field of View (FoV) offered by 360° panoramic sensors. However, due to the unique imaging process of panoramic images, models designed for pinhole images do not directly generalize satisfactorily to 360° panoramic images. In this paper, we put forward a novel network framework—PANOFLOW, to learn optical flow for panoramic images. To overcome the distortions introduced by equirectangular projection in panoramic transformation, we design a *Flow Distortion Augmentation (FDA)* method. We further propose a *Cyclic Flow Estimation (CFE)* method by leveraging the cyclicity of spherical images to infer 360° optical flow and converting large displacement to relatively small displacement. PanoFlow is applicable to any existing flow estimation method and benefit from the progress of narrow-FoV flow estimation. In addition, we create and release a synthetic panoramic dataset *Flow360* based on CARLA to facilitate training and quantitative analysis. PanoFlow achieves state-of-the-art performance. Our proposed approach reduces the End-Point-Error (EPE) on the established Flow360 dataset by 26%. On the public OmniFlowNet dataset, PanoFlow achieves an EPE of 3.34 pixels, a 53.1% error reduction from the best published result (7.12 pixels). We also validate our method via an outdoor collection vehicle, indicating strong potential and robustness for real-world navigation applications. Code and dataset are publicly available at <https://github.com/MasterHow/PanoFlow>.

## I. INTRODUCTION

One of the fundamental challenges in self-driving systems is the estimation of optical flow. Flow estimation provides information about the environment and the sensor’s motion, leading to a temporal understanding of the world, which is vital for many robotics and vehicular applications, including scene parsing, image-based navigation, visual odometry, and SLAM [1]–[6]. With the development of spherical cameras,

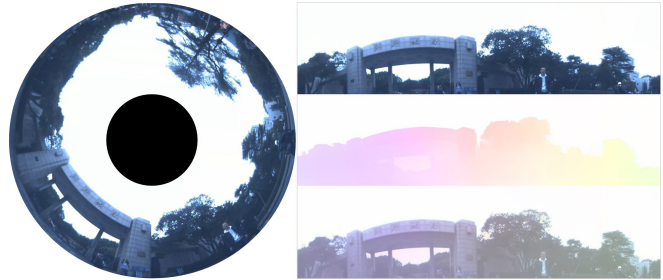


Fig. 1. Raw panoramic annular image captured by our mobile perception system and the proposed panoramic optical flow estimation on real-world surrounding view for 360° seamless scene temporal understanding.

panoramic (360°) images are now more easily captured, and can better be integrated with LiDARs due to the similar projection model [7]. However, learning-based methods have always focused on traditional 2D images produced by pinhole projection model based cameras [8]–[10]. Models designed for a camera with narrow Field-of-View (FoV) are usually sub-optimal for a comprehensive understanding. Coupling them with 360° LiDARs would also directly lead to inherent and domain adaptation problems [11]. Thus, the ability to infer optical flow of a camera’s complete surrounding has motivated the study of 360° flow estimation.

Unlike classical linear images, panoramic contents often suffer from severe distortions due to the equirectangular projection of spherical cameras [12]. An object will deform to varying degrees at different latitudes in panoramic images, making flow estimation more difficult between the target image and the attended image. Another critical issue lies in the cyclicity of spherical boundaries, which means there is more than one path from the source point to the target point, and usually there is one shorter and one longer path [13]. The two routes together form a great circle on the sphere. In other words, the geometric meanings of the two routes are equivalent. However, traditional learning-based models cannot track pixels moving outside the image boundary, and therefore have no choice but to infer the harder long-distance motion vector, leading to less satisfactory estimation.

To tackle these issues, we introduce a new panoramic flow estimation framework—PANOFLOW, to directly estimate dense flow field from panoramic images. PanoFlow is based on state-of-the-art optical flow networks [9], [10] and adapted for panoramic optical flow tasks. We present the first, to the authors’ best knowledge, a *Flow Distortion Augmentation (FDA)* method, that is built on the insight of the distortion induced by equirectangular projection, to enhance robustness against deformations in panoramic images. While distortion augmentation is used in panoramic scene parsing [14], [15], it

\*This work was partly supported by Sunny Optical Technology (Group) Co. Ltd. This work was also supported in part by the National Natural Science Foundation of China (NSFC) under Grant No. 12174341, in part by the Federal Ministry of Labor and Social Affairs (BMAS) through the AccessibleMaps project under Grant 01KM151112, in part by the University of Excellence through the “KIT Future Fields” project, and in part by Hangzhou SurImage Technology Company Ltd.

<sup>1</sup>H. Shi, Y. Ye, X. Yin, and K. Wang are with State Key Laboratory of Modern Optical Instrumentation, Zhejiang University, China {haoshi, yaozuye, xiaotingyin, wangkaiwei}@zju.edu.cn

<sup>2</sup>Y. Zhou is with Shanghai Artificial Intelligence Laboratory, China zhouyifan@pjlab.org.cn

<sup>3</sup>K. Yang is with Institute for Anthropomatics and Robotics, Karlsruhe Institute of Technology, Germany kailun.yang@kit.edu

<sup>4</sup>Z. Yin is with College of Computer Science and Technology, Zhejiang University, China pidandan@zju.edu.cn

<sup>5</sup>H. Shi and S. Meng are with Data Intelligence Lab, Luokung Technology Corp., China {shihao, mengshi}@luokung.com

<sup>†</sup>These authors contributed equally.

has not been investigated in optical flow estimation, as optical flow is a 2D vector, which incurs further challenges. By projecting participating images (attended- and target images) and flow ground truth onto the distortion field, we improve the model’s ability to generalize to deformed regions. From another distortion-adaptive perspective, we further propose to address the distortion by replacing the first layer of the encoder with a deformable convolution layer [16]. The proposed FDA and the deformable convolution empower the model to handle characteristic panoramic image distortions and robustify flow estimation. As a novel data augmentation method, FDA is a plug-and-play module for any learning-based optical flow network.

Furthermore, we design a *Cyclic Flow Estimation (CFE)* method to leverage the cyclicity of panoramic images, and convert long-distance estimation to a relatively short-distance estimation. CFE well relieves the stress of the model in large displacement estimation, enabling the model to focus on locally fine-grained optical flow estimation. CFE is a general optical flow estimation method and thus can benefit from the advances of narrow-FoV flow estimation methods.

In addition, to overcome the lack of available panoramic training data and to foster research on 360° understanding, we establish and release a new synthetic panoramic flow estimation benchmark of street scenes—*Flow360*. We generate the dataset via the CARLA simulator [17]. Flow360 consists of 6,400 color images, optical flow, and pixel-level semantic ground truth, providing an environment similar to the real world, thanks to dynamic weather, diverse city street scenes, and different types of vehicles. We use this dataset for learning to infer flow from panoramic content.

We conduct extensive quantitative experiments on the established Flow360 benchmark. Compared with the previous best model, the End-Point-Error (EPE) of PanoFlow on this dataset reduces by 26%. Further, the EPE of our approach on the public OmniFlowNet dataset [12] is reduced by 53.1% compared with the best published results (3.34 pixels vs. 7.12 pixels). Moreover, a comprehensive set of ablation experiments demonstrates the effectiveness of the proposed FDA and CFE methods. We also assemble an outdoor data collection vehicle installed with a Panoramic Annular Lens (PAL) system to validate our approach in real-world surrounding perception.

In summary, our main contributions are as follows:

- We have introduced *flow distortion augmentation*, a new data augmentation method for optical flow networks, which can help models learn to capture the motion information even on deformed regions.
- We propose a generic *cyclic flow estimation* method, which can transform large displacement estimation to relatively short displacement estimation under panoramic content.
- We generate *Flow360*, a new publicly available panoramic dataset that consists of diverse synthetic street scenes, providing both pixel-level flow- and semantic ground truth.
- Our entire framework PANOFLOW achieves state-of-

the-art performance on the established Flow360 benchmark and the public OmniFlowNet dataset.

## II. RELATED WORK

### A. Learning for 360° Flow Estimation

The classical optical flow estimation approaches [18], [19] use variational approaches to minimize energy based on brightness constancy and spatial smoothness. Since the advent of FlowNet [20], some other works based on CNN [21]–[23] have appeared. Besides, there are also some self-supervised approaches [24], [25]. Most of these methods are normally designed to work with pinhole cameras capturing a limited imaging angle. With the arrival on the market of the increasingly affordable, portable, and accurate panoramic cameras, 360° flow estimation is in urgent need, that can provide a wide-FoV temporal understanding, for which some methods based on deep learning are developed. LiteFlowNet360 [26] is designed as a domain adaptation framework to cope with inherent distortion in 360° videos caused by the sphere-to-plane projection. OmniFlowNet [12] is built on a CNN model specializing in perspective images, and it is then applied to omnidirectional ones without training on new datasets. Yuan *et al.* [13] propose a 360° optical flow estimation method based on tangent images. Differing from these works, we tackle image distortions and object deformations that appear across the entire 360° scenes and leverage the cyclicity of omnidirectional data for enhancing panoramic optical flow estimation.

### B. Panoramic Scene Understanding Datasets

Panoramic datasets are needed in a wide variety of application areas, including depth estimation [27]–[29], semantic segmentation [29], [30], and so on. The 360D dataset [11] reuses released large-scale 3D datasets and re-purposes them to 360° via rendering for dense depth estimation. PASS [14] presents a panoramic annular semantic segmentation framework with an associated dataset for credible evaluation. KITTI-360 [31] is collected with perspective stereo cameras, a pair of fisheye cameras, and a laser scanning unit for enabling 360° perception. WoodScape [32] comprises of multiple surround-view fisheye cameras and multiple tasks like segmentation and soiling detection. The OmniScape dataset [33] includes semantic segmentation, depth map, intrinsic parameters of the cameras, and the dynamic parameters of the motorcycle. Aiming at improving the accuracy of optical flow estimation, OmniFlow [34] is a synthetic omnidirectional human optical flow dataset with images of household activities with the FOV of 180°. OmniFlowNet [12] renders a test set of panoramic optical flow only for validation, using simple geometric models based on Blender. We note that, until now, there is neither a dataset for omnidirectional images targeting at outdoor complex street scenes, nor a dataset covers 360° that can be used for training and evaluation. The present paper seeks to fill this gap, by proposing a virtual environment, in which one car with panoramic camera drives under the assumption that pedestrians and vehicles move according to traffic rules.

### III. PANOFLOW: PROPOSED FRAMEWORK

For panoramic flow estimation, our approach comprises a novel *flow distortion augmentation (FDA)* method and a high-level *cyclic flow estimation (CFE)* method that can easily generalize to and work with any off-the-shelf perspective learning-based flow method. In our previous work [10], CS-Flow, based on cross-strip correlation, was proposed, which excels at capturing long-distance dependencies. Thus, CS-Flow is advantageous for processing  $180^\circ \times 360^\circ$  panoramic images. We study with CSFlow and the popular RAFT method [9] under the PanoFlow framework in detail in the experiment section. Now we elaborate the proposed framework PANOFLOW in the following subsections.

#### A. Flow Distortion Augmentation

In optics, distortion is a map projection which makes the straight lines distorted. To make our model adapt to equirectangular images, we perform radial distortion [35] on the training frames and ground-truth optical flow as a data augmentation method. Because the optical flow describes the relations of pixels which may be changed during the distortion, we cannot directly apply image distortion algorithm to optical flow. We propose a novel flow distortion algorithm.

Compared to image distortion, flow distortion should modify the optical flow field prior to applying distortion transformation and interpolation of general image distortion. The corrected flow field is obtained by subtracting the distorted terminal points  $v_t$  and initial points  $v_i$  generated by the inverse coordinate distortion function  $F'$ . The details of the algorithm are illustrated in Alg. 1.

In practice, we use the following coordinate transformation formula  $F : F(x_u, y_u) \rightarrow x_d, y_d$  to model the radial distortion [36]:

$$\begin{cases} x_d = P(r)(x_c + (x_u - x_c)), \\ y_d = P(r)(y_c + (y_u - y_c)), \end{cases} \quad (1)$$

where  $(x_c, y_c)$  is the distortion center (the intermediate point of image by default),  $(x_u, y_u)$  is the undistorted image point, and  $(x_d, y_d)$  is the distorted image point.  $P(x) = x + k_2x^2 + k_4x^4 + k_6x^6$  is a polynomial and  $r$  is the distance from  $(x_u, y_u)$  to  $(x_c, y_c)$ . In practice, we set  $k_2 = 1 \times 10^{-5}$ ,  $k_4 = 1 \times 10^{-14}$ ,  $k_6 = 1 \times 10^{-15}$ , which are empirically set and achieves reasonable augmentation effects for images of different resolutions. It is verified that FDA improves the adaptation of model by introducing the distorted images to the training data. The ablation experiment of FDA is discussed in Sec. V-C.

#### B. Definition of $360^\circ$ Flow

The spherical image does not contain any boundaries, and the coordinates are continuous in any direction on the image [12]. However, a boundary parallel to the meridian is naturally introduced in the process of unfolding the spherical image into an equirectangular image. Therefore, the cyclicity of a great circle on the sphere, is reflected in the cyclicity of the vertical boundary on the equirectangular image. Considering that the attended image and the target image, pixels

---

#### Algorithm 1 Flow Distortion

---

**Input:** Flow Field  $V$ , Coordinate Distortion Function  $F$   
**Output:** Distorted Flow Field  $V_d$

- 1:  $F' \leftarrow \text{GetInverseTransformation}(F)$
- 2:  $V_i \leftarrow \text{GenerateCoordinateGrid}(V.\text{Height}, V.\text{Width})$
- 3: **for**  $v_i, v$  in  $V_i, V$  **do**
- 4:      $v_t \leftarrow v_i + v$
- 5:      $v_i \leftarrow F'(v_i)$
- 6:      $v_t \leftarrow F'(v_t)$
- 7:      $v \leftarrow v_t - v_i$
- 8:  $V_d \leftarrow \text{ImageDistortion}(V, F)$
- 9: **return**  $V_d$

---

moving out the image boundary on one side will locate to the other side of the image. Thus, there are two 2D motion vectors that connect the source and target points: one is connected along the interior of the equirectangular image, whereas the other points outside the image boundaries. These two flow vectors together form a great circle on the spherical image, one shorter and one longer.

For the classical definition of optical flow, given two frames of sequence equirectangular RGB images  $I_1$  and  $I_2$ , we estimate the dense motion vector  $(u, v)$  from each pixel  $(x, y)$  of  $I_1$  to each pixel  $(x', y')$  of  $I_2$ , that is, the optical flow field  $V$ , which gives the per-pixel mapping relationship between the source and target. However, classical optical flow cannot track pixels that move outside the image boundaries, and cannot reflect the boundary circulation of panoramic optical flow. Following [13], we define  $360^\circ$  optical flow  $V_{360}$  as the shortest path from source to target along the great circle between them, which naturally limits the scalar value of lateral optical flow to  $u \leq 180^\circ$ . For ground-truth flow field  $(u, v)$  of equirectangular images, we can easily convert the optical flow to  $360^\circ$  flow:

$$V_{360} = \begin{cases} (u - W, v), & W/2 < u \leq W; \\ (u + W, v), & -W \leq u < -W/2; \\ (u, v), & \text{others.} \end{cases} \quad (2)$$

#### C. Cyclic Flow Estimation

In order to directly infer  $360^\circ$  Flow from equirectangular contents, and relieve the stress of the model in long-distance displacement estimation, we introduce a *Cyclic Flow Estimation (CFE)* method. The structure of CFE is shown in Fig. 2. CFE exploits the cyclicity of the left and right boundaries of equirectangular images, and it is compatible with any optical flow network based on an encoder-decoder structure, e.g., RAFT [9] or CSFlow [10].

Specifically, we first use a convolutional network as the encoder  $e(\cdot)$  to extract features  $F_1, F_2 \in \mathbb{R}^{C \times H \times W}$  from the input two frames of equirectangular images  $I_1, I_2 \in \mathbb{R}^{3 \times h \times w}$ . Then, the features are split along the horizontal centerline into  $F_{a1}, F_{b1} \in \mathbb{R}^{C \times H \times \frac{W}{2}}$  and  $F_{a2}, F_{b2} \in \mathbb{R}^{C \times H \times \frac{W}{2}}$ , respectively. We regard the process of feature encoding as rigid, that means, we should obtain exactly the same features for the same image input. Therefore, when

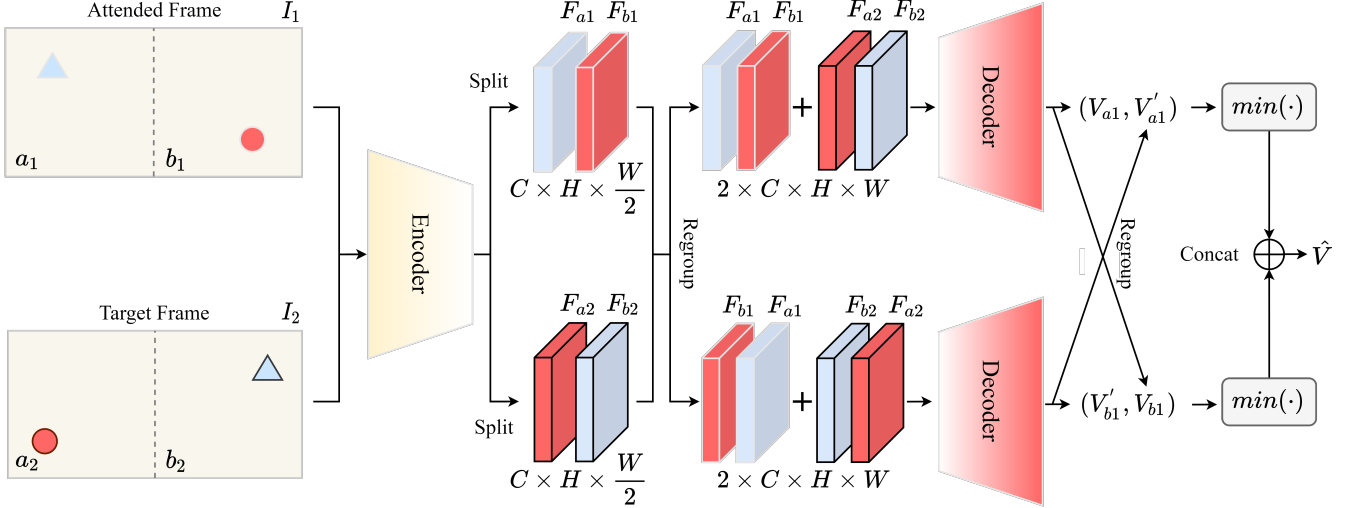


Fig. 2. *Cyclic Flow Estimation*. Partitioned feature maps are extracted from the encoder of the attended frame and the target frame. According to the cyclicity of the left and right boundaries of a panoramic image, the features extracted via the encoder, are regrouped into two feature pairs and sent to the decoder to obtain the complementary optical flow field. The  $360^\circ$  flow can finally be obtained via  $\min(\cdot)$  operations. We benefit from the assumption that the encoding process should be rigid, which allows us to eliminate redundant encoding calculations.

swapping the left and right regions of the input image, the resulting feature maps should also be approximately left-right swapped. Based on the above observations, we can regroup the feature maps as two feature pairs  $P_1, P_2 \in \mathbb{R}^{2 \times C \times H \times W}$ :

$$\begin{cases} P_1 = \{F_{a1} \oplus F_{b1}, F_{a2} \oplus F_{b2}\}, \\ P_2 = \{F_{b1} \oplus F_{a1}, F_{b2} \oplus F_{a2}\}. \end{cases} \quad (3)$$

where  $\oplus$  means a concatenate operation. Since the RAFT [9] structure contains an additional context encoder  $c(\cdot)$ , the context feature maps  $C_{a1}, C_{b1} \in \mathbb{R}^{C \times H \times \frac{W}{2}}$  which extract from  $I_1$  should also be regrouped into  $P_{c1}, P_{c2} \in \mathbb{R}^{C \times H \times W}$ :

$$\begin{cases} P_{c1} = \{C_{a1} \oplus C_{b1}\}, \\ P_{c2} = \{C_{b1} \oplus C_{a1}\}. \end{cases} \quad (4)$$

We then stack the feature pairs with context respectively, which will be further sent to the decoder  $d(\cdot)$ . The decoder will estimate two flow fields  $V, V' \in \mathbb{R}^{2 \times h \times w}$ . The flow estimations are split along the horizontal centerline into  $V_{a1}, V_{b1} \in \mathbb{R}^{2 \times h \times \frac{w}{2}}$  and  $V'_{a1}, V'_{b1} \in \mathbb{R}^{2 \times h \times \frac{w}{2}}$ . Assuming that the estimation is unbiased, for any pixel  $(x, y)$  in area  $a$ , we consider that  $V_{a1}(x, y)$  and  $V'_{a1}(x, y)$  form a pair of complementary optical flows end to end, and these two 2D motion vectors together form a great circle on the sphere. The same is true for area  $b$ . According to our definition of  $360^\circ$  optical flow, the final  $360^\circ$  flow field  $\hat{V}$  is obtained:

$$\hat{V} = \min(V_{a1}, V'_{a1}) \oplus \min(V'_{b1}, V_{b1}). \quad (5)$$

We emphasize again that CFE is a generic flow estimation method based on the assumption that the encoding process should be rigid, which can replace the large displacement estimation with the small displacement estimation when dealing with panoramic contents. Considering that large displacement estimation is much more challenging for the

model, CFE can significantly improve the accuracy of prediction. With the proposed CFE method, we eliminate redundant encoding calculations, and ensure computational efficiency while accurately estimating  $360^\circ$  optical flow. Another naive idea is to use circular convolutions to replace classical convolutional layers. However, we will demonstrate in ablation studies (Sec. V-C) that this method has a limited circularity and thus it is not suitable for panoramic flow estimation.

#### D. Deformable Receptive Field Encoder

Unlike pinhole images, equirectangular images suffer from severe geometric distortions in panoramic dense prediction [11], [14]. While our flow distortion augmentation helps address the deformations from the perspective of training data, classical CNN-based encoders are still limited by the fixed geometry of the convolution kernels, and has insufficient learning ability for deformable features. Therefore, we propose to replace the first convolutional layer of the encoder with deformable convolution [16] when dealing with  $360^\circ$  contents, endowing the model with a more flexible receptive field. In our practice, we replace the feature encoder and context encoder with two deformable convolution layers with a kernel size of  $7 \times 7$ , respectively. We will demonstrate that the use of deformable receptive field encoder further enhances the robustness of the model to distorted images.

## IV. FLOW360: ESTABLISHED SYNTHETIC DATASET

End-to-end learning of deep neural networks requires a large amount of annotated ground truth data. Although for pinhole cameras this can be partly resolved by using scanning LiDARs and multiple sensors [38], [39], such an approach is unpractical for  $360^\circ$  images, considering that panoramic camera and LiDAR will block each other and have a large diversity in their resolutions. Even when these flaws are patched using algorithms during acquisition, additional errors are still introduced. On the other hand, synthetic datasets are

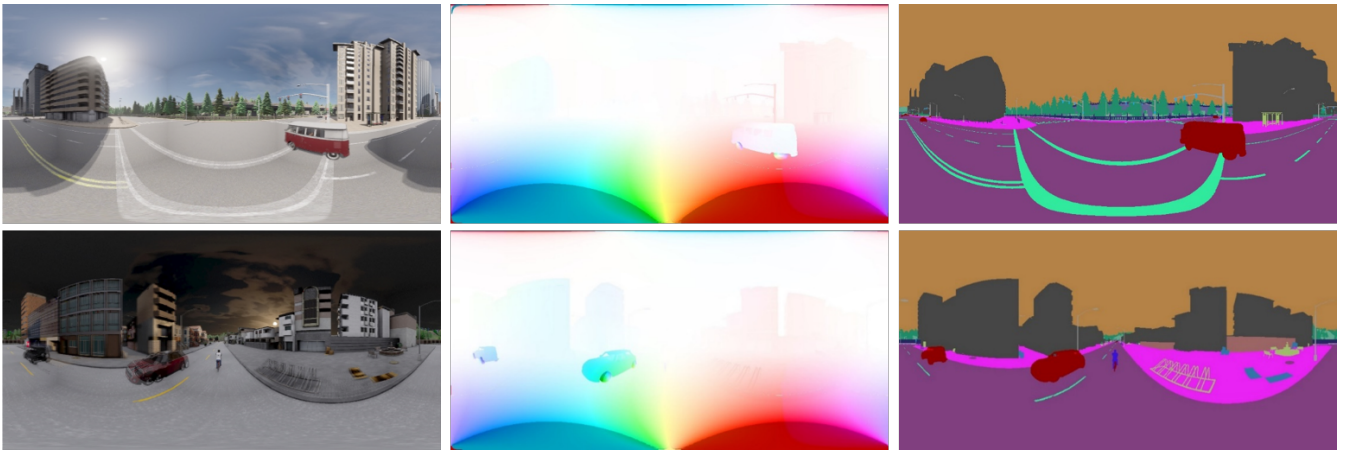


Fig. 3. From left to right: overlapping image pairs, optical flow, and semantics. The proposed *Flow360* dataset consists of 8 various city maps in four weathers: sunny, fog, cloud, and rain. We collect 100 consecutive panoramic images at each random position, resulting in a total of 6,400 frames with a resolution of  $1024 \times 512$ , each with optical flow ground truth and semantic labels, which can be used for training and evaluation. Since the flow field of panoramic images usually contains large displacement that interferes with visualization and fades colors, we modified the visualization method of optical flow based on [37], and lowered the color saturation of optical flow greater than the threshold. Please refer to our open source documentation for details.

popular for learning flow estimation due to the lack of real-world training data [20], [40], [41]. Extensive investigations have demonstrated that generalization from synthetic-to-real is feasible for optical flow tasks [9], [10], [42].

**Flow360 dataset:** We notice that there is a lack of an open panoramic optical flow dataset that can be used for training and credible numerical evaluation. Therefore, we rely on generating a dataset with ground truth flow by synthesizing both the color image and flow via the CARLA Simulator [17]. Specifically, we use eight open-source maps given by CARLA. We first use six pinhole cameras with a FoV of  $90^\circ \times 90^\circ$  at the same viewpoint to acquire a series of cube-map images  $\{I_1, I_2, \dots, I_6\} \in \mathbb{R}$ . We can then acquire the spherical image  $I_p \in \mathbb{R}$  by using a cubemap-to-equirectangular algorithm with a FoV of  $180^\circ \times 360^\circ$  [33]. We use a tracing renderer to render our dataset by placing these pinhole cameras at a random position  $P \in \mathbb{R}^3$  in the scene. For each map, we augment the dataset by changing weather, including sunny (62.5%), cloud (12.5%), fog (12.5%), and rain (12.5%) to form Flow360 and assess the robustness of optical flow estimation in various conditions. In order to ensure a good diversity of the synthetic data, we only gather 100 frames with a frame rate of  $30Hz$  for each position. Considering the unreliable optical flow at infinity such as that on points in the sky, we additionally provide ground-truth values of pixel-wise semantic segmentation for selection, which could also be beneficial for panoramic semantic understanding tasks [14], [15]. The semantic labels follow CARLA’s setting (Fig. 3). Overall, Flow360 provides 6,400 panoramic images of diverse street scenes, each with ground truth of both optical flow and semantic labels.

## V. EXPERIMENTS

We conduct experiments using two typical learning-based flow method [9], [10] to verify the proposed PanoFlow framework. Quantitative experiments show that, under the PanoFlow framework, the accuracy is improved by 26.0% on Flow360. We also confirm the role of the key components

in PanoFlow through ablation experiments. Furthermore, our approach achieves an End-Point-Error (EPE) of 3.31 pixels on Flow360, a 85.1% error reduction compared with the state-of-the-art method (22.16 pixels). On the OmniFlowNet dataset [12], PanoFlow obtains an EPE of 3.34 pixels, a 53.1% error reduction from the best published result (7.12 pixels). Additional experiments demonstrate that the computational complexity of our method is modest compared to the large performance improvement.

### A. Training Details

Following previous works, we pretrain our model using the FlyingChairs [20]→FlyThings [41] schedule, followed by finetuning on our Flow360 dataset. We divide Flow360 into 5,000/1,400 image pairs for train/test subsets. Considering that the sunny days are the most common weather, the test set of Flow360 covers sunny (57.1%), cloud (14.3%), fog (14.3%), and rain (14.3%). We train our model on an NVIDIA Tesla P40 GPU, implemented in PyTorch. We pretrain on FlyingChairs for  $100k$  iterations with a batch size of 10, then train for  $100k$  iterations on FlyingThings3D with a batch size of 6. Finally, We finetune on Flow360 with a batch size of 6 until the model converges using the weights from the pretrained model. The ablation experiment is performed with  $100k$  training iterations on Chairs, and the batch size is also 10. We time our method using an RTX 3060 GPU. The GRU iteration number is set to 12 during training and inference. We follow RAFT [9] for data augmentation. All experiments are with the same augmentations including occlusion augmentation [43], random rescale, perturb brightness, contrast-, saturation-, and hue augmentation.

### B. Results on Flow360

We evaluate PanoFlow on the Flow360 dataset using the test split. Results are shown in Tab. I, where we split the results based on the weather conditions. We term the method using the PanoFlow framework as PanoFlow (.). C+T means that the models are trained on FlyingChairs

TABLE I  
QUANTITATIVE RESULTS ON FLOW360 DATASET.

Training Data	Method	Sunny (test)	Cloud (test)	Fog (test)	Rain (test)	All (test)	Diff
		EPE	EPE	EPE	EPE	EPE	
C+T	RAFT [9]	16.57	11.16	15.04	17.00	15.64	-
	PanoFlow (RAFT)	14.93	11.25	13.88	13.36	14.03	↑ <b>10.3%</b>
	CSFlow [10]	16.32	11.16	14.99	16.04	15.35	-
	PanoFlow (CSFlow)	14.74	11.18	13.64	13.42	<b>13.89</b>	↑ <b>9.5%</b>
C+T+F	RAFT [9]	4.77	1.52	4.84	6.07	4.50	-
	PanoFlow (RAFT)	3.62	1.38	3.60	4.25	3.39	↑ <b>24.7%</b>
	CSFlow [10]	4.70	1.46	4.79	6.24	4.47	-
	PanoFlow (CSFlow)	3.56	1.47	3.56	3.94	<b>3.31</b>	↑ <b>26.0%</b>

TABLE II  
ABLATION EXPERIMENT RESULTS.

Core Components			Sunny	Cloud	Fog	Rain	All
FDA	CFE	DCN	EPE	EPE	EPE	EPE	EPE
-	-	-	18.53	12.88	17.00	18.02	17.43
✓	-	-	17.86	12.63	16.60	17.59	16.89
-	✓	-	16.56	12.46	15.25	15.35	15.62
-	-	✓	18.11	12.69	16.66	17.78	17.08
-	✓	✓	15.93	12.13	14.69	15.03	15.08
✓	-	✓	17.68	12.49	16.37	17.35	16.70
✓	✓	-	15.84	12.17	14.77	14.83	15.02
✓	✓	✓	<b>15.66</b>	<b>12.08</b>	<b>14.59</b>	<b>14.66</b>	<b>14.85</b>

TABLE III  
CYCLIC FLOW ESTIMATION ABLATION.

CFE Settings	Flow360 (test)				Avg	Diff	Time
	sunny	cloud	fog	rain			
None	4.77	<u>1.52</u>	4.84	6.07	4.50	-	<b>0.20s</b>
Circular Convolution	5.72	2.73	6.02	7.50	5.59	↓ 19.5%	<b>0.20s</b>
Double Estimation	<u>3.81</u>	1.68	3.86	<u>4.29</u>	<u>3.58</u>	↑ 20.4%	0.40s
Half Zero Padding	3.82	1.54	<u>3.74</u>	4.57	3.59	↑ 20.2%	0.60s
Half Same Padding	31.50	23.52	22.05	35.76	29.62	↓ 558.2%	<u>0.33s</u>
Default	<b>3.62</b>	<b>1.38</b>	<b>3.60</b>	<b>4.25</b>	<b>3.39</b>	↑ <b>26.0%</b>	<u>0.33s</u>

(C) and FlyingThings (T). F indicates methods using only Flow360 (F) train split for finetuning. When using C+T for training, our method achieves a 10.3% error reduction for RAFT, and a 9.5% error reduction for CSFlow. The results of CSFlow are slightly better than RAFT, which demonstrates its better cross-dataset generalizability. After finetuning on Flow360, estimating flow under PanoFlow framework can further improve the accuracy. Our PanoFlow (CSFlow) improves EPE from 4.47 to 3.31 (↑ 26.0%). It is worth noting that CSFlow outperforms RAFT in most weather, except in rainy days. This is due to the cross-strip correlation [10] that encodes the global context. The rainy data synthesized by CARLA contains a large number of similar raindrops distributed throughout the panoramic image. Therefore, while the introduction of global context via CSFlow is beneficial for most weather conditions, the fine-grained all-pair correlation in RAFT serves as an important advantage in rainy scenes.

### C. Ablation Studies

To demonstrate the role of each core module in the proposed PanoFlow framework, we perform the ablation studies on Flow360 using the well-known RAFT [9] structure. We now describe the findings of each study.

**Core Components:** Tab. II shows how performance varies as each core component (FDA: flow distortion augmentation; CFE: cyclic flow estimation; DCN: deformable receptive field encoder) of our model is removed. We can see that every component contributes to the overall performance. We

find that CFE has the greatest impact on accuracy. The result is surprising, considering that this method that can be used without any retraining. This also shows that the PanoFlow framework can easily benefit from advances in general optical flow networks. When all the key components are in place, the model performs optimally in all weathers. In the following experiments, we use the “full” version of our method (last row of Tab. II).

**Cyclic Flow Estimation:** We additionally conduct ablation study based on PanoFlow (RAFT) that has been finetuned on Flow360 to further investigate how the setting of the CFE affects the accuracy and efficiency. Tab. III shows that CFE improves the performance the most in the default setting. The best results are bolded, and the second best are underlined. **Circular Convolution:** We replaced the convolutional layers in the model with circular convolutions, where experimental results show they did not help performance. We believe that this is because the circular convolution uses a simple padding operation to warp the image, and the introduced cyclicity is insufficient, considering that the end point of the 360° optical flow may fall within the area  $[0, \frac{W}{2}]$  outside the left and right boundaries of the panoramic image. However, most of the flow vector is still given in the direction of the traditional optical flow, which makes it a disadvantage in 360° flow evaluation (↓19.5%). **Double Estimation:** A naive idea is to swap the left and right regions directly, estimate twice and take the respective minimum values. This does improve the accuracy, but the time complexity is also doubled. Due to the false image boundary introduced by the

TABLE IV  
COMPARISON WITH OMNIFLOWNET.

Method	OmniFlowNet Dataset								Flow360	
	Cartoon Tree		Forest		Low Poly		Average		Test	
	EPE	Diff	EPE	Diff	EPE	Diff	EPE	Diff	EPE	Diff
OmniFlowNet [12]	5.37	-	8.68	-	7.32	-	7.12	-	22.16	-
OmniFlowNet (RAFT)	4.84	↑ 9.9%	8.70	↑ 0.2%	6.74	↑ 7.9%	6.76	↑ 5.1%	19.61	↑ 11.5%
PanoFlow (RAFT)	3.95	↑ 26.4%	4.77	↑ 45.0%	6.78	↑ 7.4%	5.17	↑ 27.4%	14.03	↑ 36.7%
PanoFlow (RAFT) +	<u>2.31</u>	↑ 57.0%	<u>3.53</u>	↑ 59.3%	<u>4.91</u>	↑ 32.9%	<u>3.58</u>	↑ 49.8%	<u>3.39</u>	↑ 84.7%
PanoFlow (CSFlow)	3.81	↑ 29.1%	4.76	↑ 45.2%	6.92	↑ 5.5%	5.16	↑ 27.5%	13.89	↑ 37.3%
PanoFlow (CSFlow) +	<b>2.02</b>	↑ 62.4%	<b>3.51</b>	↑ 59.6%	<b>4.48</b>	↑ 38.8%	<b>3.34</b>	↑ 53.1%	<b>3.31</b>	↑ 85.1%

swap operation, it also confuses the model during encoding, leading to sub-optimal results. *Half Zero Padding*: Based on the above observations, we naturally associate whether the another region’s feature will interfere with the results of the region of interest when decoding. Thus, we try to replace half of the feature maps with empty tensors, resulting in one encoding and four decodings. We find that it has no advantages over the default setting. *Half Same Padding*: We further replace the zero feature with same feature of the region of interest. The same features make the model face two confusing scene cues at the same time when calculating the visual similarity, which leads to terrible performance regression. *Default*: The performance improvement brought by CFE is the most significant in the default setting, and its time complexity is only modest.

#### D. Comparison with the State-of-the-Art

OmniFlowNet [12] is a state-of-the-art CNN for optical flow estimation in omnidirectional images which can be built on general CNNs for perspective images. We reproduce the OmniFlowNet using MMFlow [44] and compare it with our model. Since OmniFlowNet is built on LiteFlowNet2 [45], which is inconsistent to our baseline, we also apply the architecture of OmniFlowNet to RAFT. We evaluate the models on the OmniFlowNet dataset [12] and our Flow360 dataset as shown in Tab. IV. All models are trained on FlyingChairs (C) + FlyThings (T), with “+” indicating that the model was additionally fine-tuned on the Flow360 data.

When the method of OmniFlowNet is applied to RAFT (OmniFlowNet (RAFT)), the results are improved to some extent (↑5.1% on the OmniFlowNet dataset). However, PanoFlow (RAFT) improves performance significantly (↑27.4% on the OmniFlowNet dataset). PanoFlow (CSFlow) achieves better performance than PanoFlow (RAFT) on both datasets, which proves the superiority of our CSFlow structure. After finetuning on Flow360, the accuracy of both networks is further improved, indicating that the Flow360 dataset is effective for panoramic optical flow tasks. PanoFlow (CSFlow)+ ranks 1st on the OmniFlowNet dataset (3.34 pixels), which shows that the structure of our model facilitates generalization as well. On the OmniFlowNet dataset, our approach achieves a 53.1% error reduction than the current state-of-the-art panoramic flow method. On Flow360,

TABLE V  
RUNNING TIME, PARAMETERS, AND MEMORY REQUIREMENT.

Method	Parameters	GPU Memory	Time	ΔAccuracy
RAFT [9]	5.3M	2.48GB	0.20s	-
PanoFlow (RAFT)	5.3M	2.98GB	0.33s	↑ 24.7%
CSFlow [10]	5.6M	3.23GB	0.21s	-
PanoFlow (CSFlow)	5.6M	3.73GB	0.36s	↑ 26.0%

PanoFlow (CSFlow)+ also outperforms OmniFlowNet by a large margin, decreasing EPE from 22.16 to 3.31.

#### E. Efficiency Analysis

We report the parameter counts, memory requirements during inference, inference time, and the accuracy performance as shown in Tab. V. Accuracy is determined by performance on the Flow360 (test) after training on C+T+F. The image size is  $512 \times 1024$ . RAFT takes 2.48GB memory while our approach takes 2.98GB memory. Overall, the results demonstrate that the computational overhead of PanoFlow is low compared to the significant performance improvement.

#### F. Qualitative Analysis

To investigate the practical performance of the proposed PanoFlow solution on real data, we installed a panoramic annular lens system on top of a mobile robot with an FoV of  $60^\circ \times 360^\circ$ . As shown in Fig. 4, we collected panoramic videos on the campus and compared our approach with the results given by OmniFlowNet [12]. Although the robot’s perspective and FoV are significantly different to that of the virtual camera used in the Flow360 for training, PanoFlow still gives clear and sharp optical flow estimation. Specifically, for pedestrian and fast-moving vehicles in the foreground of panoramic images, PanoFlow does not confuse them with the motion of the background, even if they are deformed to varying degrees. Edges are blurred and indistinguishable in OmniFlowNet’s background flow estimation, while the outlines of street scenes are still sharp and recognizable in PanoFlow’s results. We conclude that our method outperforms the previous state-of-the-art work for both foreground and background, showing excellent synthetic-to-real generalizability.

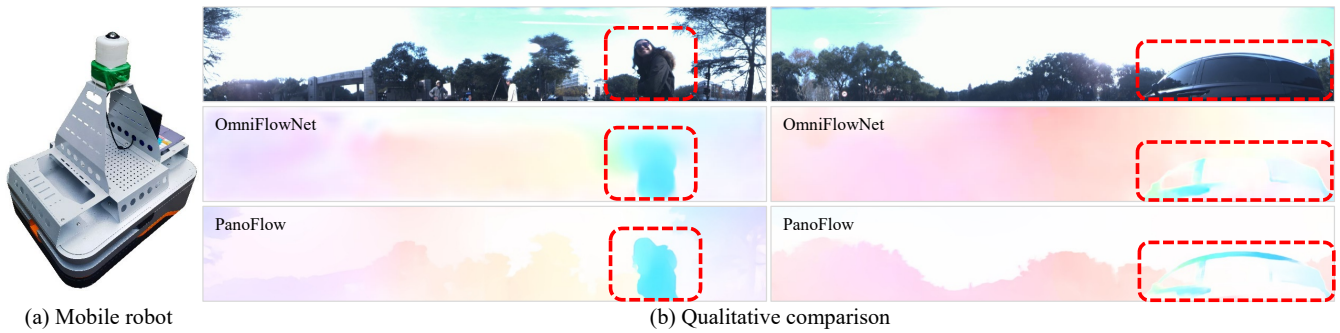


Fig. 4. (a) The mobile robot installed with a Panoramic Annular Lens (PAL) camera and a laptop, (b) Qualitative comparison with OmniFlowNet.

## VI. CONCLUSIONS

In this paper, we proposed PanoFlow, a flexible framework for estimating  $360^\circ$  optical flow using flow distortion augmentation, cyclic flow estimation, and deformable receptive field encoder. We also proposed Flow360, a publicly available synthetic panoramic optical flow dataset, which can be used for training and evaluation. We have proved through a large number of quantitative experiments that our PanoFlow is compatible with any optical flow methods of an encoder-decoder structure, which significantly improves the accuracy of panoramic flow estimation while ensuring computational efficiency. PanoFlow achieves state-of-the-art performance on all existing datasets. We look forward to further exploring the adaptability of the PanoFlow framework for other downstream panoramic tasks in the future.

## REFERENCES

- [1] R. Gadde, V. Jampani, and P. V. Gehler, "Semantic video CNNs through representation warping," in *JCCV*, 2017.
- [2] N. Hirose, F. Xia, R. Martín-Martín, A. Sadeghian, and S. Savarese, "Deep visual MPC-policy learning for navigation," *RA-L*, 2019.
- [3] D. Caruso, J. Engel, and D. Cremers, "Large-scale direct SLAM for omnidirectional cameras," in *IROS*, 2015.
- [4] X. Zhu, Y. Xiong, J. Dai, L. Yuan, and Y. Wei, "Deep feature flow for video recognition," in *CVPR*, 2017.
- [5] Z. Min, Y. Yang, and E. Dunn, "VOLDOR: Visual odometry from log-logistic dense optical flow residuals," in *CVPR*, 2020.
- [6] Z. Teed and J. Deng, "DROID-SLAM: Deep visual SLAM for monocular, stereo, and RGB-D cameras," *NeurIPS*, 2021.
- [7] J. S. Berrio, M. Shan, S. Worrall, and E. Nebot, "Camera-LIDAR integration: Probabilistic sensor fusion for semantic mapping," *T-ITS*, 2021.
- [8] D. Sun, X. Yang, M.-Y. Liu, and J. Kautz, "PWC-net: CNNs for optical flow using pyramid, warping, and cost volume," in *CVPR*, 2018.
- [9] Z. Teed and J. Deng, "RAFT: Recurrent all-pairs field transforms for optical flow," in *ECCV*, 2020.
- [10] H. Shi, Y. Zhou, K. Yang, X. Yin, and K. Wang, "CSFlow: Learning optical flow via cross strip correlation for autonomous driving," *arXiv preprint arXiv:2202.00909*, 2022.
- [11] N. Zioulis, A. Karakottas, D. Zarpalas, and P. Daras, "OmniDepth: Dense depth estimation for indoors spherical panoramas," in *ECCV*, 2018.
- [12] C.-O. Artizzu, H. Zhang, G. Allibert, and C. D'Elia, "OmniFlowNet: a perspective neural network adaptation for optical flow estimation in omnidirectional images," in *ICPR*, 2021.
- [13] M. Yuan and C. Richardt, "360° optical flow using tangent images," in *BMVC*, 2021.
- [14] K. Yang, X. Hu, L. M. Bergasa, E. Romera, and K. Wang, "PASS: Panoramic annular semantic segmentation," *T-ITS*, 2020.
- [15] K. Yang, X. Hu, H. Chen, K. Xiang, K. Wang, and R. Stiefelhagen, "DS-PASS: Detail-sensitive panoramic annular semantic segmentation through SwaftNet for surrounding sensing," in *IV*, 2020.
- [16] J. Dai *et al.*, "Deformable convolutional networks," in *ICCV*, 2017.
- [17] A. Dosovitskiy, G. Ros, F. Codevilla, A. Lopez, and V. Koltun, "CARLA: An open urban driving simulator," in *CoRL*, 2017.
- [18] B. K. Horn and B. G. Schunck, "Determining optical flow," *AI*, 1981.
- [19] B. D. Lucas and T. Kanade, "An iterative image registration technique with an application to stereo vision," in *IJCAI*, 1981.
- [20] A. Dosovitskiy *et al.*, "FlowNet: Learning optical flow with convolutional networks," in *ICCV*, 2015.
- [21] D. Tran, L. Bourdev, R. Fergus, L. Torresani, and M. Paluri, "Deep end2end voxel2voxel prediction," in *CVPRW*, 2016.
- [22] A. Ahmadi and I. Patras, "Unsupervised convolutional neural networks for motion estimation," in *ICIP*, 2016.
- [23] J. Wulff and M. J. Black, "Efficient sparse-to-dense optical flow estimation using a learned basis and layers," in *CVPR*, 2015.
- [24] P. Liu, M. Lyu, I. King, and J. Xu, "SelfFlow: Self-supervised learning of optical flow," in *CVPR*, 2019.
- [25] H.-Y. Tung, H.-W. Tung, E. Yumer, and K. Fragkiadaki, "Self-supervised learning of motion capture," *NeurIPS*, 2017.
- [26] K. Bhandari, Z. Zong, and Y. Yan, "Revisiting optical flow estimation in 360 videos," in *ICPR*, 2021.
- [27] S. Im, H. Ha, F. Rameau, H.-G. Jeon, G. Choe, and I. S. Kweon, "All-around depth from small motion with a spherical panoramic camera," in *ECCV*, 2016.
- [28] H. Jiang, Z. Sheng, S. Zhu, Z. Dong, and R. Huang, "UniFuse: Unidirectional fusion for  $360^\circ$  panorama depth estimation," *RA-L*, 2021.
- [29] C. Sun, M. Sun, and H.-T. Chen, "HoHoNet: 360 indoor holistic understanding with latent horizontal features," in *CVPR*, 2021.
- [30] K. Yang, J. Zhang, S. Reiß, X. Hu, and R. Stiefelhagen, "Capturing omni-range context for omnidirectional segmentation," in *CVPR*, 2021.
- [31] Y. Liao, J. Xie, and A. Geiger, "KITTI-360: A novel dataset and benchmarks for urban scene understanding in 2D and 3D," *arXiv preprint arXiv:2109.13410*, 2021.
- [32] S. Yogamani *et al.*, "WoodScape: A multi-task, multi-camera fisheye dataset for autonomous driving," in *ICCV*, 2019.
- [33] A. R. Sekkat, Y. Dupuis, P. Vasseur, and P. Honeine, "The OmniScape dataset," in *ICRA*, 2020.
- [34] R. Seidel, A. Aplitzsch, and G. Hirtz, "OmniFlow: Human omnidirectional optical flow," in *CVPR*, 2021.
- [35] D. C. Brown, "Decentering distortion of lenses," *PE&RS*, 1966.
- [36] A. W. Fitzgibbon, "Simultaneous linear estimation of multiple view geometry and lens distortion," in *CVPR*, 2001.
- [37] S. Baker, D. Scharstein, J. Lewis, S. Roth, M. J. Black, and R. Szeliski, "A database and evaluation methodology for optical flow," *IJCV*, 2011.
- [38] A. Geiger, P. Lenz, C. Stiller, and R. Urtasun, "Vision meets robotics: The KITTI dataset," *IJRR*, 2013.
- [39] D. Kondermann *et al.*, "The HCI benchmark suite: Stereo and flow ground truth with uncertainties for urban autonomous driving," in *CVPRW*, 2016.
- [40] D. J. Butler, J. Wulff, G. B. Stanley, and M. J. Black, "A naturalistic open source movie for optical flow evaluation," in *ECCV*, 2012.
- [41] N. Mayer *et al.*, "A large dataset to train convolutional networks for disparity, optical flow, and scene flow estimation," in *CVPR*, 2016.
- [42] H. Xu, J. Yang, J. Cai, J. Zhang, and X. Tong, "High-resolution optical flow from ID attention and correlation," in *ICCV*, 2021.
- [43] G. Yang, J. Manela, M. Happold, and D. Ramanan, "Hierarchical deep stereo matching on high-resolution images," in *CVPR*, 2019.
- [44] M. Contributors, "MMFlow: OpenMMLab optical flow toolbox and benchmark," <https://github.com/open-mmlab/mmlflow>, 2021.
- [45] T.-W. Hui, X. Tang, and C. C. Loy, "A lightweight optical flow CNN - Revisiting data fidelity and regularization," *TPAMI*, 2021.